Novel 3D silicon sensors for neutron detection

2014 JINST 9 C05001

(http://iopscience.iop.org/1748-0221/9/05/C05001)

PUBLISHED BY IOP PUBLISHING FOR SISSA MEDIALAB

RECEIVED: *January 21, 2014*
REVISED: *February 27, 2014*
ACCEPTED: *March 26, 2014*
PUBLISHED: *May 5, 2014*

15th INTERNATIONAL WORKSHOP ON RADIATION IMAGING DETECTORS
23–27 JUNE 2013,
PARIS, FRANCE

Novel 3D silicon sensors for neutron detection

R. Mendicino,[a,b,1] **M. Boscardin,**[c] **S. Carturan,**[d,e] **M. Cinausero,**[d] **G. Collazuol,**[e,b] **G.-F. Dalla Betta,**[a,b] **M. Dalla Palma,**[a,d] **F. Gramegna,**[d] **T. Marchi,**[d] **E. Perillo,**[a,b] **M. Povoli,**[a,b] **A. Quaranta,**[a,d] **S. Ronchin**[c] **and N. Zorzi**[c]

[a] *Department of Industrial Engineering, University of Trento, Via Sommarive 14, 38123 Trento, Italy*
[b] *INFN Sezione di Padova, Via Marzolo 8, 35131 Padova, Italy*
[c] *Fondazione Bruno Kessler (FBK-CMM), Via Sommarive 18, 38123 Trento, Italy*
[d] *INFN Laboratori Nazionali di Legnaro, Viale dell'Universitá 2, 35020, Legnaro (PD), Italy*
[e] *Department of Physics and Astronomy "G.Galilei", University of Padova, Via Marzolo 8, 35131 Padova, Italy*

E-mail: roberto.mendicino@unitn.it

ABSTRACT: In this paper we report a novel 3D sensor structure to be used as a neutron detector in combination with an organic converter material based on polysiloxane. The first prototypes of the proposed device are presented, with emphasis on the experimental characterization. Selected results from the functional tests (with alpha particle source and pulsed laser scans) are discussed with the aid of TCAD simulations.

KEYWORDS: Detector design and construction technologies and materials; Neutron detectors (cold, thermal, fast neutrons)

[1] Corresponding author.

doi:10.1088/1748-0221/9/05/C05001

Contents

1 Introduction

Solid state neutron detectors are an alternative to ^{3}He counter tubes (PST) of increasing interest due to the shortage of this gas [1]. The applications of sensors having spatial, temporal and energetic resolution are huge in many different fields. Among them, security, e.g. for detection of radioactive materials or explosives [2], medical imaging [3], forensics [4], and high energy and nuclear physics. Since direct detection of neutrons is not possible in silicon, hybrid structures are necessary, where neutron interactions with a converter material produce charged particles and/or scintillation light that can be detected in silicon sensors. Significant examples of these devices employ thin-film neutron converters based on Boron [^{10}B] or Lithium [^{6}Li] [5–8]. Besides the converter material, also the silicon sensor geometry has a important influence on the efficiency of the device. In this respect, several different solutions have been proposed to increase the efficiency in comparison to standard planar sensors: sensors with cylindrical or sinusoidal perforations where the holes are filled with converter material [9, 10] and devices with silicon pillars covered by boron based converter [11]. Another important concept to improve the efficiency is the stack of many sensor layers [12].

Starting from the results obtained from the development of 3D silicon sensors, which also led to production of 3D pixel sensors for the ATLAS IBL [13], we have started the HYDE project (HYbrid DEtectors for neutrons) in collaboration with the INFN Laboratori Nazionali di Legnaro (LNL). The proposed device is composed of a 3D silicon sensor coupled with a polysiloxane rubber neutron converter, which allows for neutron conversion into reaction products and, if properly doped, into scintillation light [14].

In this paper we report on the 3D sensors and their performance. Section 2 summarizes the design and fabrication issues and the main features of the converter material. In section 3 selected results from the experimental characterization (electrical and functional measurements) are reported, whereas section 4 deals with TCAD simulations that have been performed to gain deep insight into the experimentally observed characteristics.

2 Device description

2.1 3D silicon sensor

The proposed device is a perforated silicon sensor inspired to our former 3D Single-Type-Column (STC) detectors for particle physics applications [15], while featuring quite different geometrical and process details. The first prototypes here reported were mainly aimed at test purposes, so they are not optimized in several respects.

Figure 1(a) sketches a cross-section of the devices, which are fabricated on p-type high-resistivity silicon (Float Zone) wafers with 4 inch diameter and a thickness of 230 μm. Arrays of cubic cavities with a size of $200\times200\times200\,\mu\text{m}^3$ are etched by Deep Reactive Ion Etching (DRIE) on one side and doped with Phosphorus diffusion to act as junction (n^+) electrodes. The insulation between n^+ electrodes at the Si/SiO_2 interface is ensured by a uniform p-spray implantation. Like in 3D-STC detectors, planar Ohmic (p^+) regions are obtained on the opposite side by Boron implantation. They have a grid shape and are all connected to a common bulk electrode.

After the DRIE step, the high topography on the etched side does not allow photolithography to be performed with good results, since the photoresist layer obtained by spinning is not uniform enough. Hence, a special technology has been defined, allowing the cavities to be contacted on the opposite side through narrow via holes (nominal diameter of 6 or 8 μm). By doing so, a few advantages are obtained: i) the cavity side (back side) is completely available for the coupling with the converter material; ii) in case the latter is doped to produce scintillation light, an external photodetector could also be coupled to the system in order to increase the quantum efficiency; iii) the contact side (front side) is completely available for interconnection to a read-out chip. Thanks to these features, these devices are compatible with the implementation of pixel detectors for neutrons. However, at this early stage of the project, in order to ease the characterization of the hybrid detectors without the need of bump-bonding, all the cavities in the arrays are shorted together by a metal grid to obtain diode-like structures. An example of device layout is shown in figure 1(b). The die area is 1 cm^2 and the active area (with cavities) is about 0.25 cm^2. Four metal pads (2 for the anode and 2 for the cathode, for redundancy) are available at the device corners to be used for the electrical connections to the readout system.

Several device layouts have been designed, differing by some geometrical options, namely the pitch between the cavities, and the width of the p^+ regions, as indicated in figure 1(a). More details on the 3D sensor design can be found in [16].

2.2 Neutron converter

Phenyl substituted PolySiloxane (PPS) was chosen as converting material owing to its good physical and chemical properties and ease of fabrication. This material, in fact, can be easily produced in different sizes and shapes through a room temperature process. The non-cured material can be poured also in small cavities do to its low viscosity and the cross-linked material shows a very good chemical and thermal resistance, with a working range from -60 C up to 200 C and a good transparency even with high radiation doses [17, 18]. Furthermore, polysiloxane based scintillators have reached detection efficiencies as high as 70% in comparison of standard commercial plastic scintillators. PPS was synthesized at room temperature using as a precursor a vinyl terminated polydimethylco-diphenylsiloxane resin with a hydride terminated polymethylphenyl-co-

2014 JINST 9 C05001

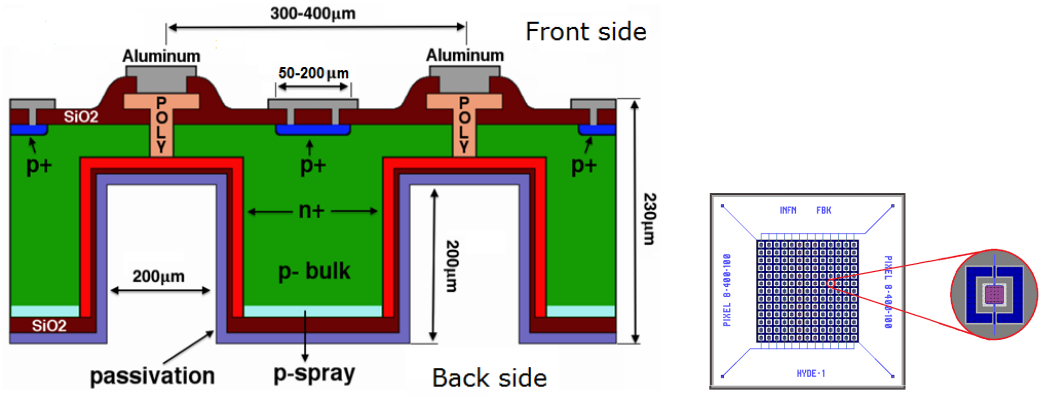

(a) (b)

Figure 1. (a) 3D sensor schematic cross-section (not to scale). (b) Sensor layout.

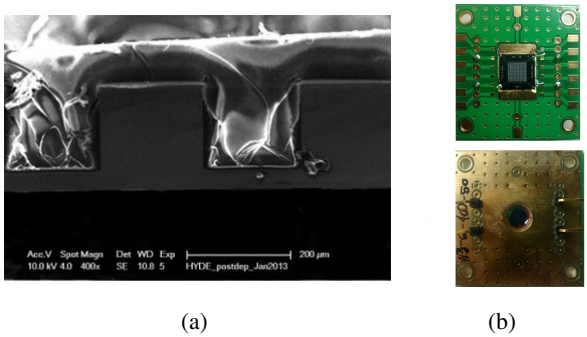

(a) (b)

Figure 2. (a) SEM photograph showing the adhesion of PPS to silicon cavities. (b) PCB board hosting a single device for functional tests (front and back).

methylhydrosiloxane resin and a platinum based catalyst [18]. The SEM photograph shown in figure 2(a) proves the good adhesion and good filling quality, with no evident voids or detachment points between the siloxane and the walls of the silicon cavities.

3 Experimental results

Results from the electrical measurements on wafer (current-voltage and capacitance-voltage) have shown a good device quality and uniformity. The leakage currents are as low as a few nA/cm^2 and the breakdown voltage is in most cases in the range from 50 V to 60 V, with only a few devices having defects that cause early breakdown. The capacitance at full depletion is of the order of 50 pF. Results of the electrical tests were confirmed from measurements on selected samples after wafer cut and assembly with custom PCB's, shown in figure 2(b). These boards have several gold plated pads for the wire bonding of the devices on the front side. A hole of $\sim$ 7 mm in diameter at the centre of the board allows exposing the array of cavities on the back side of the devices: this is useful both for functional tests and for pouring the converter material into the cavities.

Preliminary results from the detector response to fast neutrons with a broad energy spectrum (in the range from 4 to 12 MeV) and with fluxes of more than 10^6 n/(cm^{2}s), as obtained at the

2014 JINST 9 C05001

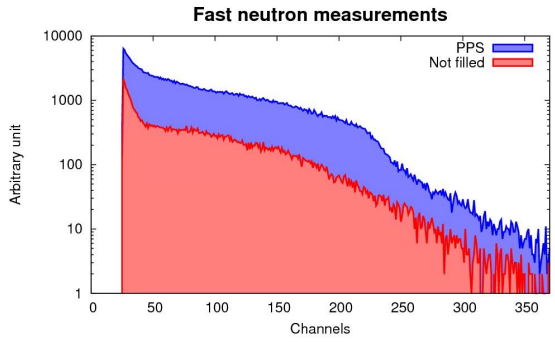

Figure 3. Fast neutrons spectra measured by two sensors, one filled with PPS and one not filled.

Isochronous Cyclotron U-120M in Rez (CZ), are shown in figure 3. Fast neutrons are obtained by the reaction of d- ions with a Be target. In order to distinguish neutron events from the gamma background, the same measurement was taken for a sensor filled with PPS and another not filled, the latter being only sensitive to gamma-rays. The same experimental setup and the same exposition time of 20 minutes were used in both cases. The clear difference between the two spectra in figure 3 can be mainly ascribed to fast neutrons converted into recoil protons by the PPS and detected by the silicon sensor. In fact, the sensitivity of the PPS to gamma-rays is intrinsically lower than the one of silicon [20]. Moreover, the gamma-ray interaction with the PPS (Compton scattering) produces electrons that have a short range in the converter, hence low probability to reach the silicon detector. As a result, gamma-rays contribute to the much higher number of counts observed with the PPS only to a minor extent.

Functional tests on the bare silicon sensors (without any converter deposition) were intended to study in detail their behaviour by emulating their working conditions when coupled to the PPS. Two types of measurement were performed. The first one makes use of α particles from a ^{241}Am source with a nominal activity of 3 kBq, and a main energy peak at 5.5 MeV, the second one is based on a position resolved pulsed laser system with different wavelengths available in the range from 635 nm to 1060 nm. For this study, we have used only the wavelengths compatible with light absorption at depths similar to the range of reaction products from PPS in silicon.

The test setup is composed of a pre-amplifier (Cremat CR110) and a shaper amplifier. For the latter either a digital version (Amptek DP4) with variable shaping times or an analog one (Cremat CR-200) with a shaping time of 4 μs were used. The output of the shaper is fed to a multichannel analyzer (MCA) (Amptek MCA8000a) to build the energy spectra (note that the MCA is embedded in the DP4 digital shaper). The laser scan setup comprises two micrometer step-to-step motors able to move the optical source in the x and y directions. The output signals of the pre-amplifier/shaper read-out chain is triggered with the signal from the laser driver.

The availability of different shapers allowing to vary the shaping time over a wide range of values proved to be very important, due to the peculiar dynamics of the output signals. Figure 4 shows an example of the spectra collected with the ^{241}Am source at two different bias voltages and two peaking times of 4 μs and 102.4 μs, respectively. The source is positioned at about 1 cm from the sensor, and α particles impinge on it from the back side. The expected charge for an α particle travelling in air for 1 cm is approximately 950 ke$^-$, and events at this charge value are

2014 JINST 9 C05001

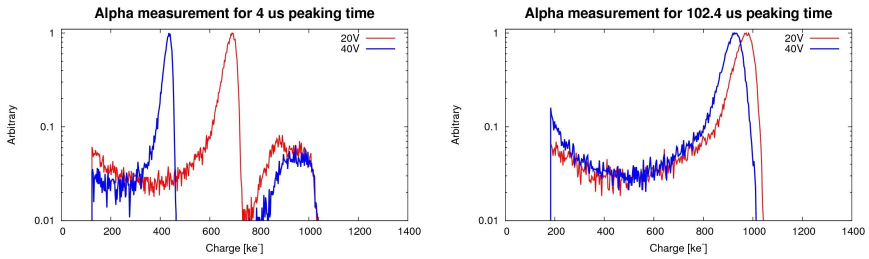

(a) (b)

Figure 4. Collected charge spectra obtained from ^{241}Am α particles impinging the 3D sensor from the back side at two bias voltages and two different peaking times: (a) 4 μs, and (b) 102.4 μs.

indeed observed in figure 4, but with clear differences depending on the shaping time. In fact, in figure 4(a) most of the events correspond to a lower charge value, and this trend is more pronounced at larger bias voltage. It should be noted that this effect is not present when the α particles impinge on the sensors from the front side: in this case the spectra, not shown, are similar to those of figure 4(b), where only one broad peak is observed, with a low influence of the voltage.

Considering the geometry of the sensor and the details of the experimental setup, analytical calculations provide a good agreement between the probability that α particles impact on the floor of the cavities and the relative number of counts at full signal charge in figure 4(a). Laser scans were also useful to better understand this effect. As an example, figure 5 shows two laser scans over a square area of 200×200 μm^2 including part of a cavity (region A) and the surrounding silicon pillar (region B). The measurements were performed with laser pulses at a wavelength of 850 nm impinging on the sensor back side. The peaking time is 4 μs and two bias voltages are considered. At 20 V, higher signals are measured from region B, as expected, because 850 nm photons are not fully absorbed in region A that is only 30 μm thick. On the contrary, a clear signal inversion can be observed at higher voltage: the signal from region A remains almost constant, whereas the signal from region B is largely reduced. Conversely, laser scans performed at 102.4 μs peaking time (not shown) are similar to that of figure 5(a), regardless of the bias voltage.

All these results can be explained by a low charge collection efficiency from the silicon pillars surrounding the cavities at low shaping times, which is further reduced at high bias voltage. This anomalous behaviour will be explained in section 4 with the aid of TCAD simulations.

4 TCAD simulations

TCAD simulations were performed with Synopsys TCAD, aiming at the study of the charge collection dynamics in response to α particles. The computation time for big and complex structures is a critical issue. The choice of the simulation domain can take advantage of the device symmetry. For functional simulations, it is necessary to account for the mutual influence between the cavities. Ideally, four quarters of four neighbour cells should be simulated. However, in order to limit the number of grid points, we focused the analysis on events relevant to two quarters, as shown in figure 6(a). In particular, four different hit positions for the α particles from the sensor back side were considered, as shown in figure 6(b).

2014 JINST 9 C05001

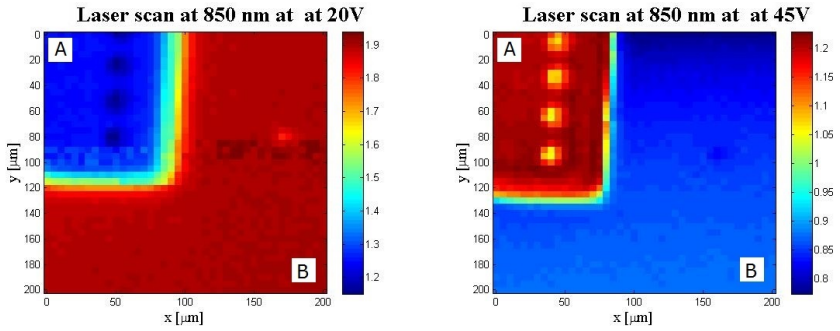

(a) (b)

Figure 5. Laser scan (wavelength 850 nm) from the sensor back side performed at 4 μs peaking time and at two different voltages: (a) 20 V , and (b) 45 V.

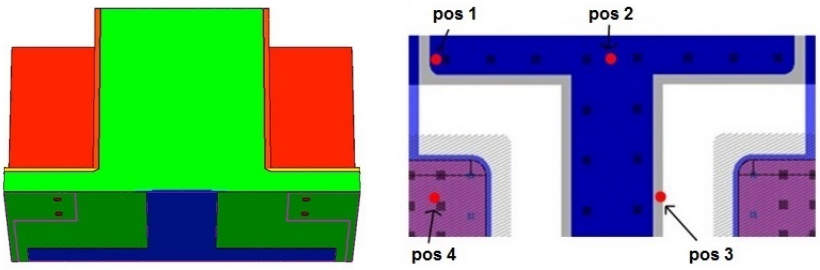

(a) (b)

Figure 6. (a) Simulation domain for functional simulations. (b) Points of incidence of alpha particle during the simulations.

Figures 7(a) and 7(b) show the output currents for the two neighbour electrodes and their sum for position 2 at 5 V and 40 V, respectively. Similar results were obtained for the other hit positions (1 and 3) within the silicon region surrounding the cavity. Due to the weighting field and electric field distributions, the fast components of the individual electrode signals have similar amplitudes but opposite polarities, so they tend to compensate one another if they are summed (note that the sum reflects what happens in a 3D diode, where all cavities are shorted). As a result, the net current has a much smaller amplitude than the two individual currents. This effect was also present in 3D-STC sensors [19], but it is here much more pronounced due to the large size of the cavities compared to the relatively narrow columnar electrodes of 3D-STC sensors.

Due to the cancellation of the fast signal components, the main contribution to the collected charge comes from the slower tails characterizing the net signals. As a result, the charge collection efficiency increases with the peaking time: it is small at 4 μs but reaches almost 100% at 102.4 μs. The compensation effect is further enhanced at higher voltage, because the fast components of the signals become more important, leading to a charge collection decrease, that is evident from figure 5. This also explains the presence of two distinct peaks at lower charge values in figure 4(a), that instead merge into one peak at higher charge at 102.4 μs peaking time, as shown in figure 4(b). The situation is quite different for hits in position 4 (i.e., the cavity floor), for which simulations

2014 JINST 9 C05001

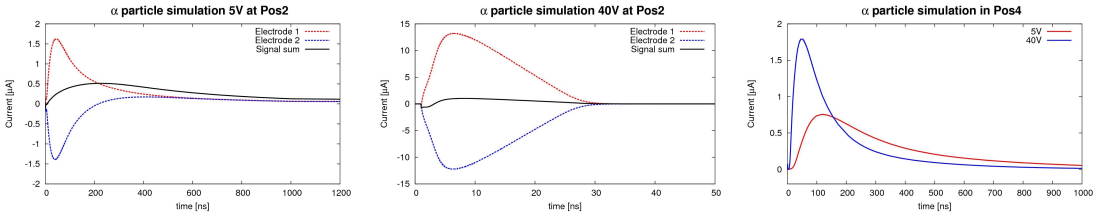

(a) (b) (c)

Figure 7. Simulated currents from two individual electrodes and their sum for α particle hit position 2 at (a) 5 V, and (b) 40 V. (c) Sum of simulated currents for α particle hit position 4 at 5 V 40 V.

show an almost 100% charge collection efficiency in all cases (see e.g. figure 7(c)). Accordingly, events relevant to this region are always observed at high charge values, regardless of the peaking time and bias voltage. Since at high peaking time most of the events relevant to different regions within the device correspond to similar (almost full) charge collection values, only one broader peak is observed in figure 4(b).

5 Conclusion

A novel 3D silicon sensor has been proposed, to be coupled to a polysiloxane converter material for the detection of fast neutrons. A dedicated technological process has been developed at FBK and a first batch of prototypes was designed and fabricated. For testing purpose, we used arrays of 3D structures shorted together and read-out as two-terminal devices (3D diodes). Preliminary tests with fast neutrons are encouraging, in spite of the low detection efficiency due to the small dimensions of the considered devices. Finally, a thorough study of the bare silicon sensor charge collection properties has been carried out, both experimentally and with the aid of TCAD simulations. The dependence of the charge collection efficiency on the bias voltage and the peaking time observed in the measurement has been fully explained with TCAD simulations, providing useful information for improving the sensor design in future productions. In particular, the optimized silicon sensors will be truly 3D (i.e., they will feature also Ohmic vertical electrodes), so that the induced signals will be very fast (a few ns) and with rising times in the order of ~ 100 ps. By doing so, it will be possible to exploit Time-of-Flight (ToF) techniques in order to discriminate gamma-rays from fast neutrons.

Acknowledgments

This work was supported in part by the Italian National Institute for Nuclear Physics (INFN) through the CSN5 project HYDE. Part of the research has been conducted at the CANAM (Center of Accelerators and Nuclear Analytical Methods LM2011019) infrastructure with a funding from the Ministry of Education, Youth and Sports of the Czech Republic. The authors are grateful to Milan Štefánik for the realization of the measurements with the cyclotron facility and Jirí Vacík, Carlos Granja and Tomas Slaviček for the helpful discussion.

2014 JINST 9 C05001

References

[1] M. Henske et al., *The ^{10}B based Jalousie neutron detector — An alternative for ^{3}He filled position sensitive counter tubes*, *Nucl. Instrum. Meth.* **A 686** (2012) 151.

[2] R. T. Kouzes et al., *Neutron detection alternatives to ^{3}He for national security applications*, *Nucl. Instrum. Meth.* **A 623** (2010) 1035.

[3] M Strobl et al., *Advances in neutron radiography and tomography*, *J. Phys.* **D 42** (2009) 243001.

[4] Z. Vargaa and G. Surányi, *Detection of previous neutron irradiation and reprocessing of uranium materials for nuclear forensic purposes*, *Appl. Radiat. Isot.* **67** (2009) 516.

[5] D.S. McGregor et al., *Design considerations for thin film coated semiconductor thermal neutron detectors - I: basics regarding alpha particle emitting neutron reactive films*, *Nucl. Instrum. Meth.* **A 500** (2003) 272.

[6] T.C. Unruh et al., *Design and operation of a 2-D thin-film semiconductor neutron detector array for use as a beamport monitor*, *Nucl. Instrum. Meth.* **A 604** (2009) 150.

[7] J. Uher et al., *Characterization of 3D thermal neutron semiconductor detectors*, *Nucl. Instrum. Meth.* **A 576** (2007) 32.

[8] R. Nikolic et al., *Silicon-based, pillar-structured thermal-neutron detectors*, *SPIE Newsroom* (2010).

[9] J.K. Shultis and D.S. McGregor, *Design and performance considerations for perforated semiconductor thermal-neutron detectors*, *Nucl. Instrum. Meth.* **A 606** (2009) 608.

[10] S.L. Bellinger et al., *Variant Designs and Characteristics of Improved Microstructured Solid-State Neutron Detectors*, *IEEE Nucl. Sci. Symp. Conf. Rec. (NSS/MIC)* **2009** (2009) 986.

[11] D.S. McGregor et al., *Microstructured semiconductor neutron detectors*, *Nucl. Instrum. Meth.* **A 608** (2009) 125.

[12] S.L. Bellinger et al., *Enhanced variant designs and characteristics of the microstructured solid-state neutron detector*, *Nucl. Instrum. Meth.* **A 652** (2011) 387.

[13] C. Da Via et al., *3D silicon sensors: Design, large area production and quality assurance forthe ATLAS IBL pixel detector upgrade*, *Nucl. Instrum. Meth.* **A 694** (2012) 321.

[14] A. Quaranta et al., *Optical and scintillation properties of polydimethyl-diphenylsiloxane based organic scintillators*, *IEEE Trans. Nucl. Sci.* **57** (2010) 891.

[15] C. Piemonte et al., *Development of 3D detectors featuring columnar electrodes of the same doping type*, *Nucl. Instrum. Meth.* **A 541** (2005) 441.

[16] M. Dalla Palma et al., *Hybrid Detectors for Neutrons Combining Phenyl-Polysiloxanes with 3D Silicon Detectors*, *IEEE ANIMMA* **2013** (2013) 1.

[17] M. Bowen et al., *New radiation-resistant plastic scintillator*, *IEEE Trans. Nucl. Sci.* **36** (1989) 562.

[18] A. Quaranta et al., *Characterization of polysiloxane organic scintillators produced with different phenyl containing blends*, *Mater. Chem. Phys.* **137** (2013) 951.

[19] A. Zoboli et al., *Electro-optical measurements of 3D-stc detectors fabricated at ITC-irst*, *Nucl. Instrum. Meth.* **A 583** (2007) 149.

[20] http://www.nist.gov/pml/data/xcom/index.cfm.

2014 JINST 9 C05001